Structural and Magnetic Studies of Cr³⁺ Substituted Nickel Ferrite Nanomaterials Prepared by Sol-Gel Auto-Combustion

Jinpei Lin [1,2,†], Yun He [1,3,†], Xianglin Du [1], Qing Lin [1,2,*] , Hu Yang [1] and Hongtao Shen [1,4,*]

[1] Guangxi Key Laboratory of Nuclear Physics and Nuclear Technology, Guangxi Normal University, Guilin 541004, China; linjinpei.2007@163.com (J.L.); hy@mailbox.gxnu.edu.cn (Y.H.); linqinglab@126.com(X.D.); yanghu000@126.com (H.Y.)

[2] College of Medical Informatics, Hainan Medical University, Haikou 571199, China

[3] Sate Key Laboratory for Chemistry and Molecular Engineering of Medicinal Resources, Guangxi Normal University, Guilin 541004, China

[4] College of Physics and Technology, Guangxi Normal University, Guilin 541004, China

* Correspondence: hy@gxnu.edu.cn (Q.L.); heyunlab@163.com (H.S.)

† These authors contributed equally to this work.

check for updates

Abstract: The present study envisages the preparation of chromium substituted Nickel ferrite $NiCr_xFe_{2-x}O_4$ ($x = 0\sim1.0$) powders by a sol-gel auto-combustion method. X-ray diffraction analysis (XRD) showed that the specimens with $x > 0.2$ exhibited a single-phase spinel structure, and that more content of Cr within a specimen is favorable for the synthesis of pure Ni-Cr ferrites. The lattice parameter decreased with an increase in the Cr concentration. The sample without calcining exhibited a good crystallinity. Scanning Electron Microscopy (SEM) showed the formation of ferrite powders nano-particles, and that the substitution of Cr weakened the agglomeration between the particles. Mössbauer spectra of $NiCr_xFe_{2-x}O_4$ showed two normal Zeeman-split sextets that displayed a ferrimagnetic behavior. Furthermore, the spectra indicated that iron was in the Fe^{3+} state, and the magnetic hyperfine field at the tetrahedral tended to decrease with an increase in the Cr substitution. The saturation magnetization decreased by the Cr^{3+} ions, and reached a minimum value (Ms = 4.46 emu/g). With an increase in the annealing temperature, the coercivity increased initially, which later decreased.

Keywords: Ni-Cr-ferrite; sol-gel; structure; Cr substitution; Mössbauer; magnetic properties

1. Introduction

Nickel ferrite ($NiFe_2O_4$) is a typical soft magnetic ferrite, making it one of the most important spinel ferrites [1]. It is widely used in electronic devices, due to its ability to remain permeable at high frequencies, high electrical resistivities, low eddy currents, and low dielectric losses, as well as its continuous chemical stability [2,3]. $NiFe_2O_4$ is an inverse spinel ferrite, in which the Ni^{2+} ions occupy octahedral (B) sites, and Fe^{3+} ions are distributed in tetrahedral (A) and octahedral (B) sites [2]. The magnetic and electric properties of the spinel ferrites depend on the distribution of the cations among tetrahedral and octahedral sites. Chromium ions, with an antiferromagnetic nature, are known for achieving control over magnetic parameters, and in the development of technologically important materials. Patange et al. investigated the cation distribution and magnetic properties of chromium-substituted nickel ferrite, and found that Cr^{3+} and Ni^{2+} ions both have strong preference to occupy octahedral (B) site, and the magnetic saturation and Curie temperature all decrease by Cr^{3+} ions substitution [1]. Lee et al. studied the electrical and magnetic properties of ferrite $NiCr_xFe_{2-x}O_4$,

which established that the magnetic moment and Curie temperature decreased with the chromium substitution, and that this system exhibited n-type semi-conductivity [4]. Prasad et al. prepared nanoparticles $NiCr_xFe_{2-x}O_4$ by sol-gel, and concluded that the magnetization and coercivity decreased with an increase in the chromium ion concentration, due to the depletion of Fe^{3+} ions at the octahedral (B) sites [5]. Patange et al. obtained the cation distribution of nickel chromium ferrites by the IR spectra analysis [6]. The current paper deals with structural and magnetic properties of ferrite $NiCr_xFe_{2-x}O_4$ ($x = 0~1.0$) powders that were prepared by a sol-gel auto-combustion method. The ferrite powders, prepared by this method exhibited a good sinterability with a homogeneous composition. The other advantages of the synthetic method include the requirement of relatively simple equipment, and low cost of the materials used. From previous studies [4–6], it is evident that increasing the substitution of Cr is favorable for the synthesis of pure Ni-Cr ferrites, and weakens the agglomeration between the particles.

2. Experimental

2.1. Sample Preparation

Chromium-substituted Nickel ferrite $NiCr_xFe_{2-x}O_4$ ($x = 0~1.0$) powders were synthesized using the sol-gel auto-combustion process. The raw materials were analytical grade $Ni(NO_3)_2 \cdot 6H_2O$, $Cr(NO_3)_3 \cdot 9H_2O$, $Fe(NO_3)_3 \cdot 9H_2O$, $C_6H_8O_7 \cdot H_2O$ (citric acid) and $NH_3 \cdot H_2O$ (ammonia). The molar ratio of metal nitrates to citric acid was taken as 1:1. The metal nitrates and citric acid were weighed and dissolved in deionized water to prepare the test solutions. The pH value of metal nitrate solution was adjusted from 7 to 9 by ammonia addition. The mixed solutions were heated in a thermostat water bath at 80 °C and stirred continuously to form the dried gel. Continuous dropwise addition of citric acid occurred in this process. The gels were dried in an oven at 120 °C for 2 h and were burnt in self-propagating combustion to form loose powder by being ignited in air at room temperature. The powders then were ground and sintered at temperatures of 400 °C and 800 °C.

2.2. Characterization

The crystalline structure was analyzed using X-ray diffraction (D/max-2500V/PC, Rigaku, Tokyo, Japan), with Cu Kα radiation ($\lambda = 0.15405$ nm). The micrographs were obtained by scanning electron microscopy (NoVaTM Nano SEM 430, FEI Corporation, Hillsboro, OR, USA). The Mössbauer spectrum was performed at room temperature, using a conventional Mössbauer spectrometer (Fast Com Tec PC-mossII, Oberhaching, Germany), in constant acceleration mode. The γ-rays were provided by a ^{57}Co source in a rhodium matrix. Magnetization measurements were carried out with super conducting quantum interference device (MPMS-XL-7, Quantum Design, San Diego, CA, USA) at room temperature.

3. Results and Discussion

3.1. X-ray Diffraction (XRD) Analysis

Figure 1 shows the XRD patterns of $NiCr_xFe_{2-x}O_4$ ($x = 0~1.0$) ferrites calcined at 800 °C for 3 h. XRD results show that the specimens with $x > 0.2$ exhibited a single-phase spinel structure, while an impurity peak of Fe_2O_3 was detected in the samples with $x = 0$ to 0.2. The results show that increasing the content of Cr was favorable for the synthesis of pure Ni-Cr ferrites. Similar results are evident in earlier studies [7]. Table 1 indicates that the lattice parameter showed a decreased trend, with an increasing substitution of Cr^{3+} ions. The decrease in the lattice parameter was likely due to the replacement of larger Fe^{3+} ions (0.645 Å), by smaller Cr^{3+} ions (0.63 Å) [4,8]. The average crystallite size of the investigated samples that was estimated by the Scherrer's formula [5], were found to be between 25.5 and 57.5 nm (Table 1). It was observed that the average crystallite size decreased by increasing the Cr content, as evident with earlier reports [9].
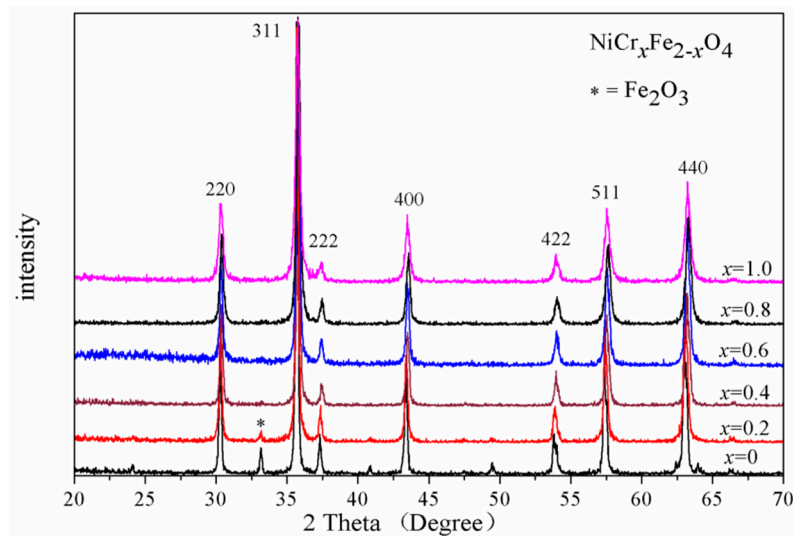
Figure 1. XRD patterns of NiCrxFe2−xO4 calcined at 800 °C.

The X-ray density was calculated using the relation [10]:

$$\rho_x = \frac{8M}{Na^3} \tag{1}$$

where M is relative molecular mass, N is the Avogadro's number and 'a' is the lattice parameter. Table 1 shows that the X-ray density highlighted a decreasing trend for Cr^{3+} concentration for all samples. The atomic weight of Fe is greater than Cr, so the relative molecular mass decreased with an increase in the Cr concentration. The decrease in the X-ray density is attributed to the fact that the relative molecular mass decreases significantly with a negligible decline in the lattice parameter.

Table 1. XRD data of NiCrxFe2−xO4 calcined at 800 °C.

Content (x)	Lattice Parameter (Å)	Average Crystallite Size (Å)	Density (g/cm^3)
0	8.34062	575	5.3664
0.2	8.33600	446	5.3562
0.4	8.31862	453	5.3735
0.6	8.31741	375	5.3581
0.8	8.30992	308	5.3548
1.0	8.31979	255	5.3179

The X-ray patterns of NiCr$_{0.2}$Fe$_{1.8}$O$_4$ calcined at different temperature are shown in Figure 2. XRD patterns confirmed the formation of cubic spinel phase as the main phase along with traces of the secondary phase of Fe$_2$O$_3$. The intensity of Fe$_2$O$_3$ decreased with increasing heating temperatures. Furthermore, it was evident that the heat treatment was favorable for the synthesis of pure Ni-Cr ferrites. The lattice parameter and the X-ray density differed with a change in temperature for the samples. Average crystallite size of NiCr$_{0.2}$Fe$_{1.8}$O$_4$ increased with increasing the calcining temperature, as evident from Table 2. In earlier work [11], the diffraction peaks of Ni$_{0.50}$Cu$_{0.25}$Zn$_{0.25}$Cr$_x$Fe$_{2-x}$O$_4$ calcined at low temperature were not very sharp, but our results indicate that the diffraction peaks of CoCr$_{0.2}$Fe$_{1.8}$O$_4$ without burning were very sharp. We prepared chromium substituted cobalt ferrite powders by the sol-gel auto-combustion method, whereas the samples without calcining showed a good crystallinity.
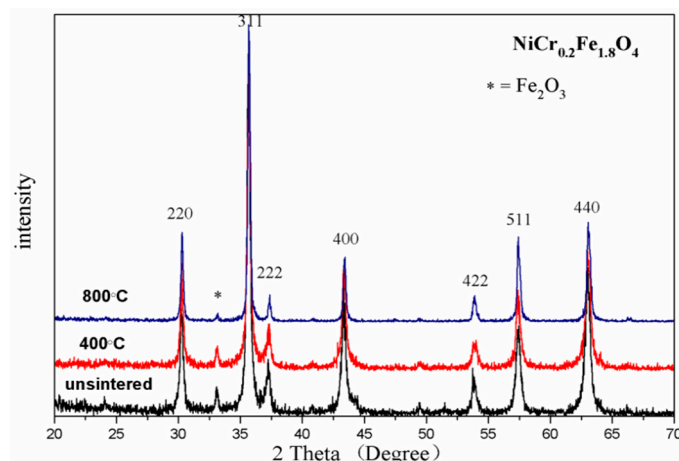
Figure 2. XRD patterns of $NiCr_{0.2}Fe_{1.8}O_4$ sintered at different temperatures.

Table 2. XRD data of $NiCr_{0.2}Fe_{1.8}O_4$ sintered at different temperatures.

Temperature (°C)	Lattice Parameter (Å)	Average Crystallite Size (Å)	Density (g/cm³)
unsintered	8.34459	293	5.3411
400 °C	8.34400	300	5.3424
800 °C	8.36000	446	5.3562

3.2. Structures and Grain Size

The Scanning Electron Microscopy (SEM) results of $NiCr_xFe_{2-x}O_4$ (x = 0, 0.2) annealed at 800 °C for 3 h is shown in Figure 3. It can be observed that the distribution of grains was almost uniform in size, and were well crystallized for all samples. The substitution of Cr can weaken the agglomeration between the particles. The histogram of grain size distribution of $NiCr_xFe_{2-x}O_4$ ferrites is shown in Figure 4 shows. The average grain size of $NiFe_2O_4$ and $NiCr_{0.2}Fe_{1.8}O_4$ estimated using a statistical method was approximately 69.51 and 52.63 nm, respectively. This shows that the ferrite powders were nano-particles, and the average grain size decreased significantly with an increase in the Cr content. The average grain size was slightly larger than the average crystallite size, as determined by XRD analysis. The data reveals that every particle was formed by a number of crystallites.
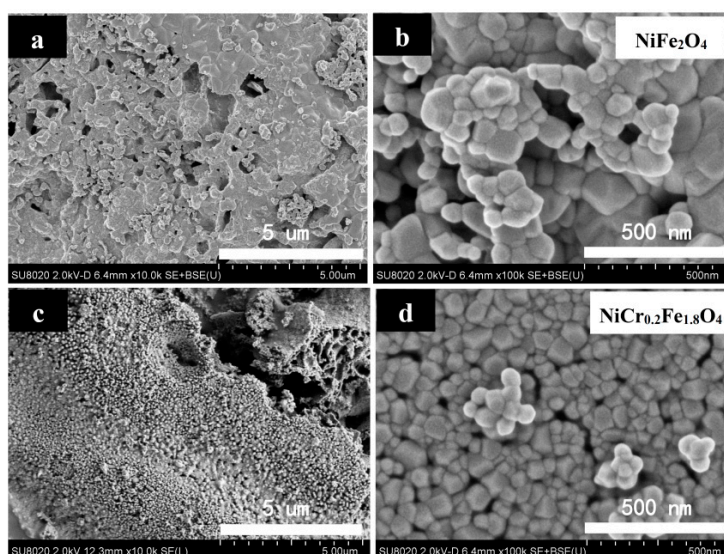

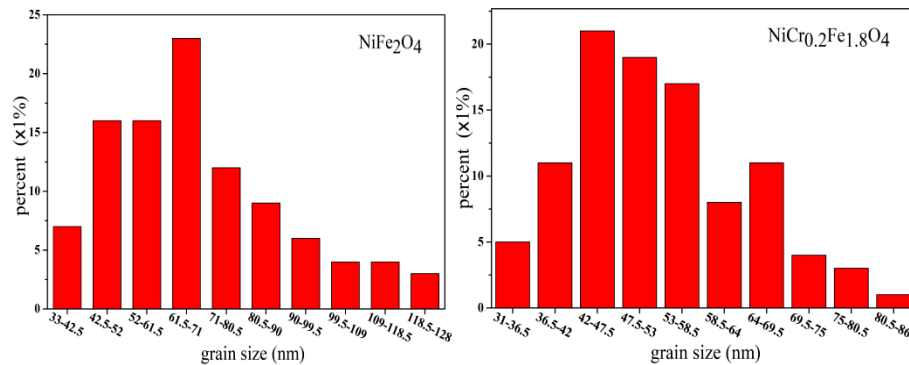**Figure 3.** SEM micrographs of $NiFe_2O_4$ and $NiCr_{0.2}Fe_{1.8}O_4$ sintered at 800 °C.

Figure 4. Histogram of grain size distribution of $NiFe_2O_4$ and $NiCr_{0.2}Fe_{1.8}O_4$.

3.3. Mössbauer Spectroscopy

The Mössbauer spectra for $NiCr_xFe_{2-x}O_4$, recorded at room temperature, is shown in Figure 5. All samples were analyzed using the Mösswinn 3.0 program. The spectra exhibited two normal Zeeman-split sextets due to the presence of Fe^{3+} at tetrahedral and octahedral sites, which indicated the ferromagnetic behavior of the samples [12]. The sextet with the larger isomer shift was assigned to the Fe^{3+} ions at the B site, and the one with the smaller isomer shift was assumed to arise from the Fe^{3+} ions, occupying the A site. This may be attributed to the difference in Fe^{3+}-O^{2-} internuclear separations. Since, the bond separation for the B site Fe^{3+} ions, was larger in comparison with the A site ions, small overlapping of the orbits for Fe^{3+} and O^{2+} ions at B site occurred, resulting in the smaller covalency and large isomer shift for B site Fe^{3+} ions [9]. It is reported that the values of Isomer Shift (I.S.) for Fe^{2+} ions lie in the range 0.6–1.7 mm/s, while for Fe^{3+} they lie in the range 0.1–0.5 mm/s [13]. From Table 3, the values for I.S. in our study indicate that iron is in Fe^{3+} state.
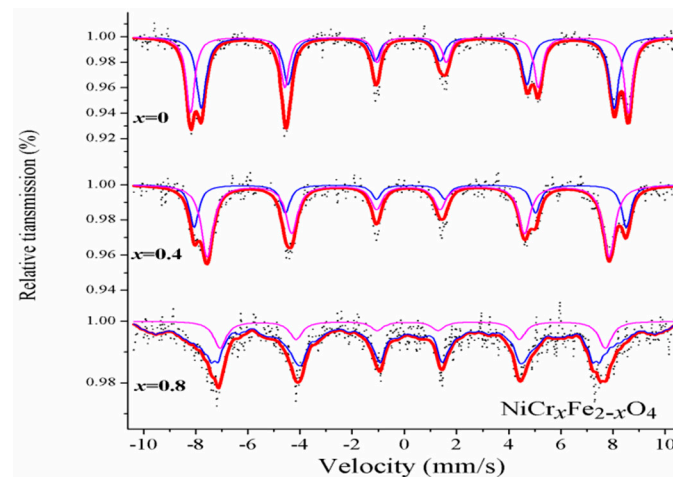

Figure 5. Mössbauer spectra of $NiCr_xFe_{2-x}O_4$ calcined at 800 °C.

Table 3 shows that the magnetic hyperfine field at the tetrahedral A site, and octahedral B site, exhibited a decreasing trend with increasing Cr substitution. The decrease of magnetic hyperfine field with increasing Cr contents is attributed to the decrease of the A-B super-exchange interaction with the magnetic Fe^{3+} ions replaced by magnetic Cr^{3+} ions, which resulted in the decrease of the magnetic hyperfine field [9]. Furthermore, the reduction of magnetic hyperfine field was related to the disappearance of the impurity Fe_2O_3. The decrease of Fe_2O_3 (with valence state $- Fe^{3+}$) led to the decrease of the superexchange interaction [14]. The quadrupole shift of Mössbauer spectra was nearly zero in our study, which indicated that the ferrites exhibited a cubic symmetry. The decrease in the absorption area ration of B site can be attributed to the Fe^{3+} ions decrease at B site, with the Cr^{3+} ions doping.

Table 3. Mössbauer parameters of $NiCr_xFe_{2-x}O_4$ calcined at 800 °C.

Content (*x*)	Component	Isomer Shift (I.S.) (mm/s)	Quadrupole Shift (Q.S.) (mm/s)	H(T)	Line Width (Γ) (mm/s)	Relative Area (A$_0$) (%)
0	Sextet (A)	0.124	0.003	48.089	0.439	51.7
	Sextet (B)	0.235	−0.087	52.051	0.384	48.3
0.4	Sextet (A)	0.146	−0.003	47.786	0.544	68.3
	Sextet (B)	0.230	−0.014	51.359	0.429	31.7
0.8	Sextet (A)	0.147	−0.219	43.373	0.352	80.2
	Sextet (B)	0.224	0.191	45.820	0.587	19.8

3.4. Magnetic Property of Particles

Figure 6 shows the hysteresis loops of $NiCr_xFe_{2-x}O_4$ at room temperature. The magnetization of all samples nearly reached a saturation point at the external field of 5000 Oe. As shown in Table 4, the saturation magnetization decreased with an increase in the Cr content.
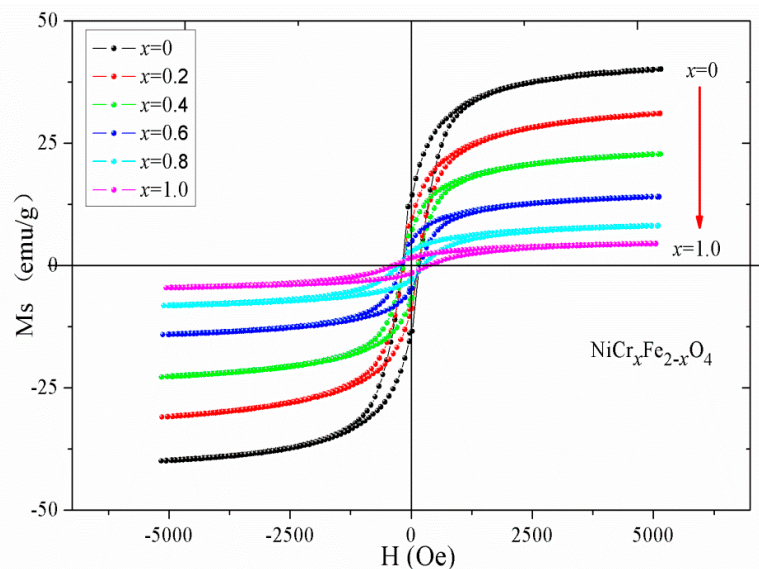
Figure 6. Hysteresis loops of $NiCr_xFe_{2-x}O_4$ calcined at 800 °C.

The saturation magnetization can be expressed by means of the following relation [4,14]:

$$\sigma_s = \frac{5585 \times n_B}{M} \tag{2}$$

where n_B is the magnetic moment with Bohr magneton as the unit, and M is the relative molecular mass. The relative molecular mass of $NiCr_xFe_{2-x}O_4$ decreased as the Cr content in x increased. The change of magnetic moment nB can be explained with Néel's theory. The magnetic moment μ per ion for Cr^{3+}, Ni^{2+} and Fe^{3+} ions was 3 μ$_B$, 2 μ$_B$ and 5 μ$_B$ [2,3,14], respectively. According to Néel's two sublattice model of ferrimagnetism, the cation distribution of $(Fe)A[NiCr_xFe_{1-x}]BO_4$ was used, since Ni^{2+} prefers to occupy the octahedral (B) site in $NiFe_2O_4$ ferrite of inverse spinel structure [1,2], and Cr^{3+} ions have strong B-site preference [3,13,14]. The magnetic moment nB is expressed as [3,4,10,14]:

$$n_B = M_B - M_A = 2 + 3\,x + 5\,(1-x) - 5 = 2 - 2x \tag{3}$$

where M_B and M_A are the B and A sublattice magnetic moments. Formula (3) shows that the theoretical magnetic moment decreases when there is an increase in the Cr content. According to the relation of Formula (2), the theoretical saturation magnetization decreased with Cr content x. The variation of the experimental and theoretical saturation magnetization agreed with each other for all samples.

Table 4. Magnetic data for $NiCr_xFe_{2-x}O_4$ calcined at 800 °C.

Content (x)	Ms (emu/g)	Hc (Oe)	Mr (emu/g)
0	40.12	177.25	13.64
0.2	31.02	152.09	9.06
0.4	22.87	154.61	6.94
0.6	14.06	185.70	4.80
0.8	8.11	253.79	2.87
1.0	4.46	361.83	1.55

It is observed from Table 4 that the coercivity of $NiCr_xFe_{2-x}O_4$ initially decreased, then subsequently increased—with an increase in the Cr content x. The coercivity was found to decrease which can be attributed to the decrease of magnetocrystalline anisotropy, as Cr has a negative magnetocrystalline anisotropy [15]. However, the coercivity increased when $x \geq 0.4$, due to influence by many factors, such as impurity phase, crystallinity, microstrain, magnetic particle morphology and size distribution, anisotropy, and magnetic domain size [16–18].

The magnetic hysteresis loops at room temperature for unsintered $NiCr_{0.2}Fe_{1.8}O_4$, and after annealing at 400 °C, 600 °C, and 800 °C, are shown in Figure 7. Table 5 indicates that $NiCr_{0.2}Fe_{1.8}O_4$ after annealing at 800 °C offered a maximum saturation magnetization value, since the particle size increased with an increase in the annealing temperature [17]. The saturation magnetization of $NiCr_{0.2}Fe_{1.8}O_4$ decreased after annealing at 400 °C and 600 °C, which may be due to the presence of an impurity phase [19,20]. Similar studies have been reported in the literature [21,22].
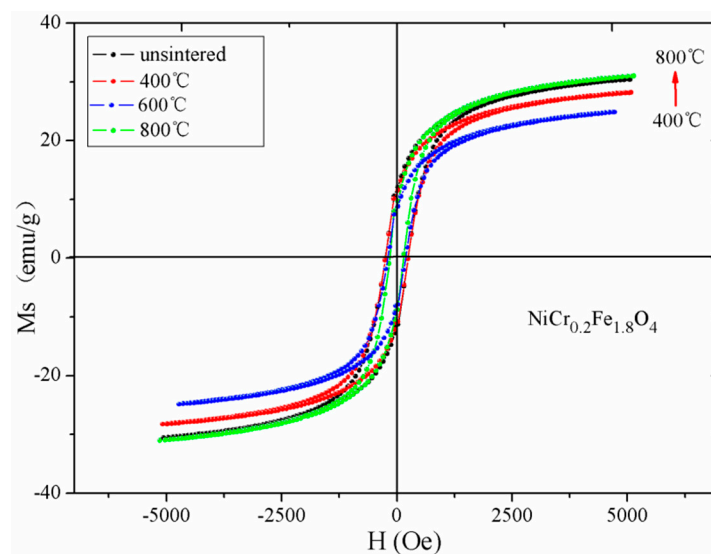
Figure 7. Hysteresis loops of $NiCr_{0.2}Fe_{1.8}O_4$ calcined at different temperatures.

The coercivity of $NiCr_{0.2}Fe_{1.8}O_4$ increased initially and subsequently decreased, with an increase in the annealing temperature. This can be explained by the variation of the grain size. The coercivity in the single domain region is expressed as $H_C = g - h/D^2$. In the multidomain region the variation of the coercivity with grain size can be expressed as in $H_C = a + b/D$, where g, h, a, and b are constants and D is the diameter of the particle [17,18]. Hence, in the single domain region, the coercivity increased with an increase in the grain size, while in the multidomain region the coercivity decreased as the particle diameter increased. In our earlier research, the grain size increased by increasing the sintered temperatures obtained by SEM. The grain size of $NiCr_{0.2}Fe_{1.8}O_4$ calcined at different temperature should be ideally from the single domain region to the multidomain region, so the coercivity increased initially and then decreased with an increase in the annealing temperature [19,20]. Moreover, the

impurity phases of Fe_2O_3 in the ferrite nanopowders is also the important factor that results in the decreases of coercivity [23–25].

Table 5. Magnetic data for $NiCr_{0.2}Fe_{1.8}O_4$ calcined at different temperatures.

Temperature (°C)	Ms (emu/g)	Hc (Oe)	Mr (emu/g)
unsintered	30.47	247.03	11.62
400 °C	28.19	247.45	11.10
600 °C	24.87	207.85	6.25
800 °C	31.02	152.09	9.06

4. Conclusions

XRD analysis of the $NiCr_xFe_{2-x}O_4$ ferrite reveals that the specimens with $x > 0.2$ exhibit a single-phase spinel structure, while the impurity peak of Fe_2O_3 was detected in the samples with x = 0 or 0.2. The decrease in the lattice parameter was probably due to the replacement of the larger Fe^{3+} ions by smaller Cr^{3+} ions. The XRD patterns of $NiCr_{0.2}Fe_{1.8}O_4$ calcined at different temperature indicate the intensity of Fe_2O_3 decreased with increasing the heat treatment temperatures, and the diffraction peaks of the sample without burning were very sharp along with a good crystallinity. SEM results indicate that the grains were distributed homogeneously, and the ferrite powers were nano-particles; the average grain size was slightly larger than the average crystallite size determined by XRD, which shows that every particle is formed by a number of crystallites. Room temperature Mössbauer spectra of $NiCr_xFe_{2-x}O_4$ calcined at 800 °C showed the presence of two normal Zeeman-split sextets, and that it exhibited a ferrimagnetic behavior for the all samples. The decrease in the magnetic hyperfine field with increasing Cr contents was attributed to the decrease of the A-B super-exchange interaction. The saturation magnetization decreased with an increase in the Cr content x, which could be explained by Néel's theory. Furthermore, with an increase in the annealing temperature, the coercivity increased initially and subsequently decreased for $NiCr_{0.2}Fe_{1.8}O_4$, since the particle size increased with increasing the annealed temperature.

Author Contributions: J.L. and Y.H. contributed equally to this work. Q.L. and Y.H. conceived and designed the experiments; Q.L. and J.L. performed the experiments; J.L. and H.S. analyzed the data; X.D. and H.Y. contributed reagents/materials/analysis tools. Q.L. and H.S. are co-corresponding authors contributed equally to this study. All authors commented and edited on the manuscript. No potential conflict of interest was reported by the authors.

Conflicts of Interest: The authors declare no conflict of interest.

References

1. Patange, S.M.; Shirsath, S.E.; Jadhav, S.S.; Lohar, K.S.; Mane, D.R.; Jadhav, K.M. Rietveld refinement and switching properties of Cr^{3+} substituted $NiFe_2O_4$ ferrites. *Mater. Lett.* **2010**, *64*, 722–724. [CrossRef]
2. He, Y.; Lei, C.; Lin, Q.; Dong, J.; Yu, Y.; Wang, L. Mössbauer and Structural properties of La-substituted $Ni_{0.4}Cu_{0.2}Zn_{0.4}Fe_2O_4$ nanocrystalline ferrite. *Sci. Adv. Mater.* **2015**, *7*, 1809–1815. [CrossRef]
3. Anh, L.N.; Duong, N.P.; Loan, T.T.; Nguyet, D.T.T.; Hien, T.D. Synchrotron and Magnetic Study of Chromium-Substituted Nickel Ferrites Prepared by Using Sol-Gel Route. *IEEE Trans. Magn.* **2014**, *50*, 1–5.
4. Lee, S.H.; Yoon, S.J.; Lee, G.J.; Kim, H.S.; Yo, C.H.; Ahn, K.; Lee, D.H.; Kim, K.H. Electrical and magnetic properties of $NiCr_xFe_{2-x}O_4$ spinel ($0 \leq x \leq 0.6$). *Mater. Chem. Phys.* **1999**, *61*, 147–152. [CrossRef]
5. Prasad, A.S.; Dolia, S.N.; Pareek, S.P.; Samariya, A.; Sharma, P.K.; Dhawan, M.S. Sol-gel synthesized high anisotropy magnetic nanoparticles of $NiCr_xFe_{2-x}O_4$. *J. Sol-Gel Sci. Technol.* **2013**, *66*, 372–377. [CrossRef]

6. Patange, S.M.; Shirsath, S.E.; Toksha, B.G.; Jadhav, S.S.; Shukla, S.J.; Jadhav, K.M. Cation distribution by Rietveld, spectral and magnetic studies of chromium-substituted nickel ferrites. *Appl. Phys. A* **2009**, *95*, 429–434. [CrossRef]

7. Xia, A.; Liu, S.; Jin, C.; Chen, L.; Lv, Y. Hydrothermal $Mg_{1-x}Zn_xFe_2O_4$ spinel ferrites: Phase formation and mechanism of saturation magnetization. *Mater. Lett.* **2013**, *105*, 199–201. [CrossRef]

8. Iqbal, M.J.; Siddiquah, M.R. Electrical and magnetic properties of chromium-substituted cobalt ferrite nanomaterials. *J. Alloys Compd.* **2008**, *453*, 513–518. [CrossRef]

9. Chae, K.P.; Lee, Y.B.; Lee, J.G.; Lee, S.H. Crystallographic and magnetic properties of $CoCr_xFe_{2-x}O_4$ ferrite powders. *J. Magn. Magn. Mater.* **2000**, *220*, 59–64. [CrossRef]

10. Singhal, S.; Jauhar, S.; Singh, J.; Chandra, K.; Bansal, S. Investigation of structural, magnetic, electrical and optical properties of chromium substituted cobalt ferrites ($CoCr_xFe_{2-x}O_4$, $0 \leq x \leq 1$) synthesized using sol gel auto combustion method. *J. Mol. Struct.* **2012**, *1012*, 182–188. [CrossRef]

11. Bayoumy, W.A.; Gabal, M.A. Synthesis characterization and magnetic properties of Cr-substituted NiCuZn nanocrystalline ferrite. *J. Alloys Compd.* **2010**, *506*, 205–209. [CrossRef]

12. Lin, Q.; Lei, C.; He, Y.; Xu, J.; Wang, R. Mössbauer and XRD studies of $Ni_{0.6}Cu_{0.2}Zn_{0.2}Ce_xFe_{2-x}O_4$ ferrites By Sol-Gel auto-combustion. *J. Nanosci. Nanotechnol.* **2015**, *15*, 2997–3003. [CrossRef] [PubMed]

13. Kumar, S.; Farea, A.M.M.; Batoo, K.M.; Lee, C.G.; Koo, B.H.; Yousef, A.; Alimuddin. Mössbauer studies of $Co_{0.5}Cd_xFe_{2.5-x}O_4$ ($0.0 \leq x \leq 0.5$) ferrite. *Phys. B Condens. Matter.* **2008**, *403*, 3604–3607. [CrossRef]

14. Toksha, B.G.; Shirsath, S.E.; Mane, M.L.; Patange, S.M.; Jadhav, S.S.; Jadhav, K.M. Autocombustion High-Temperature Synthesis, Structural, and Magnetic Properties of $CoCr_xFe_{2-x}O_4$ ($0 \leq x \leq 1.0$). *J. Phys. Chem. C* **2011**, *115*, 20905–20912. [CrossRef]

15. Gabal, M.A.; Al Angari, Y.M.; Al-Agel, F.A. Synthesis, characterization and magnetic properties of Cr-substituted Co-Zn ferrites Nanopowders. *J. Mol. Struct.* **2013**, *1035*, 341–347. [CrossRef]

16. Jiang, T.; Yang, Y.M. Effect of Gd substitution on structural and magnetic properties of Zn-Cu-Cr ferrites prepared by novel rheological technique. *Mater. Sci. Technol.* **2009**, *25*, 415–418. [CrossRef]

17. Singhal, S.; Barthwal, S.K.; Chandra, K. XRD, magnetic and Mössbauer spectral studies of nano size aluminum substituted cobalt ferrites ($CoAl_xFe_{2-x}O_4$). *J. Magn. Magn. Mater.* **2006**, *306*, 233–240. [CrossRef]

18. Harzali, H.; Marzouki, A.; Saida, F.; Megriche, A.; Mgaidi, A. Structural, magnetic and optical properties of nanosized $Ni_{0.4}Cu_{0.2}Zn_{0.4}R_{0.05}Fe_{1.95}O_4$ ($R = Eu^{3+}$, Sm^{3+}, Gd^{3+} and Pr^{3+}) ferrites synthesized by co-precipitation method with ultrasound irradiation. *J. Magn. Magn. Mater.* **2018**, *460*, 89–94. [CrossRef]

19. He, Y.; Yang, X.; Lin, J.; Lin, Q.; Dong, J. Mössbauer spectroscopy, Structural and magnetic studies of Zn^{2+} substituted magnesium ferrite nanomaterials prepared by Sol-Gel method. *J. Nanomater.* **2015**, *2015*, 854840. [CrossRef]

20. Kumar, A.; Shen, J.; Yang, W.; Zhao, H.; Sharma, P.; Varshney, D.; Li, Q. Impact of Rare Earth Gd^{3+} Ions on Structural and Magnetic Properties of $Ni_{0.5}Zn_{0.5}Fe_{2-x}Gd_xO_4$ Spinel Ferrite: Useful for Advanced Spintronic Technologies. *J. Supercond. Novel Magn.* **2018**, *31*, 1173–1182. [CrossRef]

21. Lin, L.Z.; Tu, X.Q.; Wang, R.; Peng, L. Structural and magnetic properties of Cr-substituted NiZnCo ferrite Nanopowders. *J. Magn. Magn. Mater.* **2015**, *381*, 328–331.

22. Cao, C.; Xia, A.; Liu, S.; Tong, L. Synthesis and magnetic properties of hydrothermal magnesium–zinc spinel ferrite powders. *J. Mater. Sci. Mater. Electron.* **2013**, *24*, 4901–4905. [CrossRef]

23. Li, L.Z.; Zhong, X.X.; Wang, R.; Tu, X.Q.; Peng, L. Structural and magnetic properties of Co-substituted NiCu ferrite nanopowders. *J. Magn. Magn. Mater.* **2017**, *433*, 98–103. [CrossRef]

24. Lin, J.; He, Y.; Lin, Q.; Wang, R.; Chen, H. Microstructural and Mössbauer spectroscopy Studies of $Mg_{1-x}Zn_xFe_2O_4$ (*x* = 0.5, 0.7) nanoparticles. *J. Spectrosc.* **2014**, *2014*, 540319. [CrossRef]

25. Lv, H.; Zhang, H.; Zhang, B.; Ji, G.; He, Y.; Lin, Q. A proposed electron transmission mechanism between Fe^{3+}/Co^{2+} and Fe^{3+}/Fe^{3+} in the spinel structure and its practical evidence in quaternary $Fe_{0.5}Ni_{0.5}Co_2S_4$. *J. Mater. Chem. C* **2016**, *4*, 5476–5482. [CrossRef]